

Chemical Interaction Between MgO Support and Iron Catalyst

M. Palizdar^{*1,2}, Z. Aslam², R. Aghababazadeh³, A. Mirhabibi^{2,4}, P. Sangpour⁵, Z. Abadi⁵, Y. Palizdar⁵ and R. Brydson²

* palizdar@cpg-gmbh.de

Received: November 2018

Revised: April 2019

Accepted: May 2019

¹ R&D and Training Department, CPG Industrial, Mining and Technical Services, Germany.

² Institute for Materials Research, Leeds University, U.K.

³ Institute for Color Science and Technology, Iran.

⁴ Centre of Excellence for Advanced Materials and Processing, Iran University of Science and Technology, Iran.

⁵ Advanced Materials and Nanotechnology Department, Materials and Energy Research Center, Iran.

DOI: 10.22068/ijmse.16.4.1

Abstract: In this paper, the chemical interaction between catalyst and support was studied to understand the observed different growth rate of CNTs in our previous paper. Both pure MgO and $\text{Mg}(\text{NO}_3)_2 \cdot 6\text{H}_2\text{O}$ as sources of the MgO catalyst support and $\text{Fe}_2(\text{SO}_4)_3 \cdot x\text{H}_2\text{O}$ as the source of the Fe catalyst, were employed. A Fe catalyst supported on MgO was synthesized using the wet impregnation method followed by calcination. To compare the catalyst grain size and its distribution, the sample were characterized by scanning electron microscopy (SEM), transmission electron microscopy (TEM), X-ray powder diffraction (XRD), BET specific surface area (SSA) measurement, and X-ray photoelectron spectroscopy (XPS). XPS technique was utilized complementary to demonstrate the existence of chemical interaction between MgO support and Fe catalyst. Results revealed that the type of precursor used to prepare the support had a significant influence on the morphology of the support and the associated distribution of the Fe catalysts. The highest yield of MgFe_2O_4 phase was obtained using a pure MgO precursor which after calcination resulted in a homogenous distribution of nano-sized Fe particles over the support surface.

Keywords: Catalyst, Support, Magnesium ferrite.

1. INTRODUCTION

Iijima initially reported carbon nanotubes (CNTs) in 1991[1] and due to their unusual theoretical mechanical and electrical properties, CNTs have been the subject of much experimental interest [2,3]. Laser vaporization [4], arc discharge [5], and chemical vapor deposition (CVD) [6-9] are three main synthesis methods to synthesize CNTs. CVD is acknowledged as a reliable commercial method to grow CNTs, due to advantages of low cost and high yield. In addition, it is easy to control the growth rate using the CVD method by changing the synthesis conditions such as temperature, time of growth, catalyst, catalyst-support, and hydrocarbon precursor.

Catalytic chemical vapor deposition (CCVD) is a particular case of the CVD method in which a gaseous hydrocarbon as a source of carbon is decomposed on the metal catalyst component

at high temperature [10,11] from which CNTs then grow. The quality and quantity of the CNTs produced are affected by the type, grain size, and distribution of the catalyst and the support. Transition metals such as Fe, Co, Ni, Cr, V, and Mo have been reported as catalysts while MgO, Al_2O_3 , SiO_2 , CaO, and ZrO_2 have been widely used as supports [12-14]. It is evident that these types of catalysts have been widely used not only due to the high diffusion rate of carbon but also high solubility of carbon in these metals [15,16]. Catalysts particles play the main role to achieve the chemical equilibrium between carbon-containing molecules and graphene-type materials [17]. In addition, same catalyst particles behave differently on different kinds of support materials [18]. CNTs quality and quantity are greatly influenced by the surface morphology and textural properties of support. In order to control the distribution of catalyst particles on the surface of the

support, some factors such as the porosity of the support, the optimum amounts of catalyst as well as the interaction between catalysts and support need to be considered [17-20]. Porosity increases the surface area allowing more catalyst particles to be supported. An optimum amount of catalyst in addition to surface porosity prevents potential agglomeration of catalyst particles, while interactions between catalyst and support govern the distribution of catalyst particles and its stability [15,16] which affects the quality and quantity of the CNTs produced [20,26].

In the previous paper we have shown that by using two different sources in order to synthesize a MgO support i.e. pure-MgO and $\text{Mg}(\text{NO}_3)_2 \cdot 6\text{H}_2\text{O}$, different yields of CNTs were obtained [27]. MgO is widely used as support materials in CCVD method considering its high surface area, mesoporous texture morphology, and good hardness [28]. In previous works, both pure MgO and $\text{Mg}(\text{NO}_3)_2 \cdot 6\text{H}_2\text{O}$ were used as source to synthesis MgO precursors in place of supports [29-35]. However, in our previous study, we reported that a higher yield was obtained by using a MgO precursor which had a surface hydroxide component, rather than by using calcined magnesium nitrate to synthesize MgO [27]. Use of the MgO precursor resulted in the production of long and clean bundles of single-wall nanotubes (SWNTs) and double-wall nanotubes (DWNTs) with diameters ranging between 1 and 5 nm. However, use of $\text{Mg}(\text{NO}_3)_2 \cdot 6\text{H}_2\text{O}$ produced substrates resulted in low amounts of mainly short bundles of DWNTs with diameters ranging from 3 to 5 nm [27]. Hence, we postulate that the precursor used to produce the support has a significant influence on the morphology of the support and consequently on the obtained CNTs. This paper studies the chemical interaction between catalyst particles and support which is synthesized by using different sources for MgO precursors.

2. EXPERIMENTAL DETAILS

Two different types of support precursors, MgO (Aldrich 99.99%) and $\text{Mg}(\text{NO}_3)_2 \cdot 6\text{H}_2\text{O}$ (Aldrich 99.99%), were employed to synthesize two series of supported catalysts. Wet impregnation methods were used to prepare the supported catalysts as explained previously [27,36-39].

2.1. Series A

Stoichiometric amounts of micron size MgO and $\text{Fe}_2(\text{SO}_4)_3 \cdot 7\text{H}_2\text{O}$ precursors were used as the source for support and Fe catalyst materials, respectively. They were added to 20 mL of de-ionized water to form a solution in proportions so as to achieve the desired metal loading (Fe:MgO) of 10%, which had previously been determined to be the optimum. The solution was then stirred at 80 °C for 12 h. Finally, the dried mixture was ground and then introduced to the furnace and calcined in air at 900 °C for 1 hour.

2.2. Series B

A similar method was used as for series A. However, instead of using pure-MgO as a precursor to prepare the support, as an alternative, $\text{Mg}(\text{NO}_3)_2 \cdot 6\text{H}_2\text{O}$ was used.

For both series A and B, the supported catalyst materials were characterized by scanning electron microscopy (SEM) using a Zeiss Leo FEG-SEM (Carl Zeiss SMT Ltd., Cambridge, U.K.), transmission electron microscopy (TEM) using FEI Tecnai TF20 FEG-TEM, X-ray powder diffraction XRD using a PANalytical XPert MPD system (Almelo, the Netherlands) and BET specific surface area (SSA) measurement. Also, an X-ray photoelectron spectroscopy (XPS) instrument equipped with an Al- K_α x-ray source at energy of 1486.6 eV was employed to characterize the surface chemical composition of films. The hemispherical energy analyzer (Specs EA 10 Plus) operating in a vacuum better than 10^{-7} Pa was used for binding energy analysis. All binding energy values were calibrated by fixing the C(1s) core level to the 285.0 eV. All of peaks were deconvoluted using SDP software (version 4.1) with 80% Gaussian-20% Lorentzian peak fitting.

3. RESULTS AND DISCUSSIONS

3.1. The Support

The morphologies of the support after calcination of the pure-MgO and $\text{Mg}(\text{NO}_3)_2 \cdot 6\text{H}_2\text{O}$ at 900 °C for 1 hour, were shown in our earlier work [27]. Although the XRD results for the calcined supports revealed that their crystallo-

graphic structures were similar, the morphologies were different. The SEM results showed that calcination of the pure-MgO resulted in almost uniform particles ranging between 50 and 100 nm in diameter including some elongated particles, whereas calcination of the nitrate ($\text{Mg}(\text{NO}_3)_2 \cdot 6\text{H}_2\text{O}$) caused both large, plate-like and fine particle agglomerates [27].

The main function of the support is to provide a high surface area for a stable dispersion of the metal catalyst, which then can provide a high rate of CNT growth. Hence, a more uniform morphology could result in a better CNT yield, in agreement with previous data [27]. The BET specific surface area of the calcined pure-MgO precursor was $12.48 \text{ m}^2/\text{g}$ whilst the BET specific surface of the calcined magnesium nitrate precursor was $11.12 \text{ m}^2/\text{g}$. This suggests that the particle agglomeration occurred more after calcination of the nitrate in comparison with magnesium oxide. However, the difference between the surface areas is not significant enough to obtain such a big difference in CNT quality and yield [22-27].

3.2. The Catalyst and Support

The XRD data is presented in Figure 1 for the samples from both series A and B after calcination at 900°C for 1 hour. Both results suggest the existence of magnesium oxide and magnesium ferrite following calcination. Iron oxides could be formed after sintering at 900°C for 1 hour, in both series A and B samples. However, there is no evidence for Bragg diffractions due to $\alpha\text{-Fe}_2\text{O}_3$ and, owing to the overlap between the MgO and $\gamma\text{-Fe}_2\text{O}_3$ Bragg diffraction; it is difficult to rule out the presence of $\gamma\text{-Fe}_2\text{O}_3$. However, Ning et al [25] have reported that due to the reactivity of iron oxide with MgO at high temperature, no iron or iron oxide particles remain. The mechanism of MgFe_2O_4 formation via the solid-state reaction between MgO and Fe_2O_3 has been discussed extensively [25,40-45]. In the hot, reducing atmosphere during the catalytic CVD process, it is expected that the MgFe_2O_4 particles are directly reduced to a metallic iron catalyst [25,26].

The intensity ratio between the most intense ferrite, MgFe_2O_4 and MgO peaks in the series A sample is ca. 0.132, whereas it is only ca. 0.064

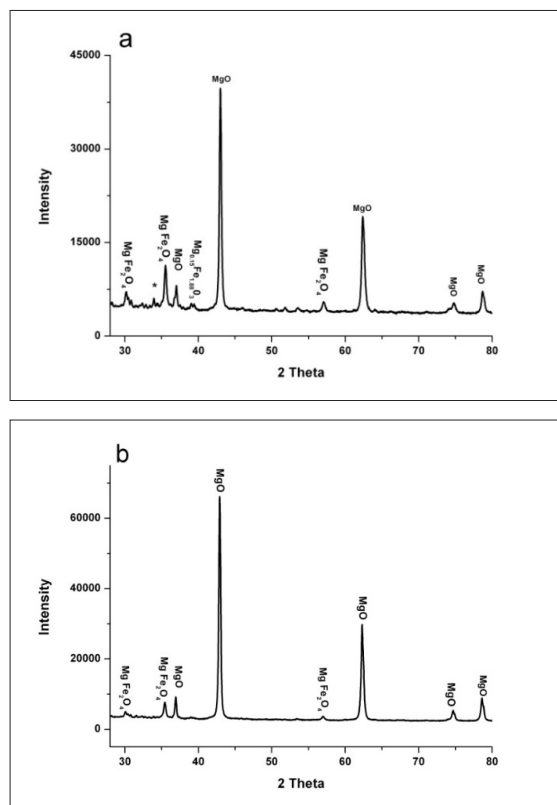


Fig. 1. (a) The X-ray diffraction pattern for series A sample consisting of a MgO precursor and iron sulfate, and (b) for series B sample consisting of an $\text{Mg}(\text{NO}_3)_2 \cdot 6\text{H}_2\text{O}$ precursor and iron sulfate, both calcined at 900°C for 1 hour.

for the series B sample, i.e. approximately half that of series A. These ratios suggest that more ferrite phase is achieved after calcination of the pure-oxide precursor (series A) in comparison with the nitrate precursor (series B). As reported elsewhere [46], the intense ferrite peaks could be caused by a textured structure and preferential crystallite orientation. However, this can be ruled out since all ferrite peaks are more intense in Fig.1-a in comparison with Fig.1-b confirming that there is no influence of texture. Thus ferrite formation appears more likely when using a MgO precursor as compared to magnesium nitrate.

It has been reported that interdiffusion between Fe catalyst particles and the MgO support could improve the dispersion of the Fe particles on the support substrate by forming a solid solution of $\text{MgFe}_2\text{O}_4/\text{MgO}$ at the metal/support interface

[25]. Due to the existence of more ferrite phase in calcined series A samples (Fig. 1-a), the dispersion of the Fe catalyst particles would, therefore, be expected to be more homogeneous (and perhaps more stable) in comparison with calcined series B samples. This prediction would agree with the results of CNT growth obtained in our previous work which showed that a higher yield of smaller CNTs was produced on MgO [27].

Fig. 2 compares the differential thermal analysis (DTA) results at a heating rate of $5^{\circ}\text{C min}^{-1}$ in air, for both series A and B samples following calcination at 900°C for 1 hour. Fig. 3a indicates two main thermal events occur during the heating process. The first is a broad endothermic peak between 100°C and 150°C due to the release of H_2O from the sample (H_2O probably is absorbed from the atmosphere). The second peak appears around 400°C which represents the dehydration of the

hydroxide $\text{Mg}(\text{OH})_2$ [47]. A comparison between Fig. 2a and Fig. 2b reveals approximately similar behavior. Series B however, exhibits a splitting in both endothermic peaks possibly due to the presence of the hydrated nitrate which decomposes to the metal oxide at ca. 450°C (in addition to adsorbed water and hydroxides). In addition, the required enthalpy for dehydration in the series B is four times larger than in the series A.

Decomposition of iron sulfate involves three main steps including the release of water from the crystalline structure, decomposition of $\text{FeO} \cdot \text{HSO}_4$ to $\text{Fe}_2\text{O}(\text{SO}_4)_2$ ($\approx 490^{\circ}\text{C}$), and finally, the thermal decomposition of FeSO_4 and $\text{Fe}_2\text{O}(\text{SO}_4)_2$ to Fe_2O_3 and $\text{SO}_2 + \text{O}_2$ at $\approx 600^{\circ}\text{C}$ [48]. However, Fig. 2 does not obviously reflect these endothermic peaks, most probably due to the overlap with the decomposition of the Mg precursor and also the low amount of iron sulfate present.

TEM results for the calcined series A sample (Fig. 3) show a good dispersion of Fe particles with little evidence of agglomeration, suggesting that the predominance of the MgFe_2O_4 phase results in a more homogenous as well as fine Fe particle distribution over the support surface. The average Fe particle size and standard deviations are 48 nm and 9 nm, respectively.

In comparison, Fig. 4 shows TEM images for the calcined catalyst/support prepared from the $\text{Mg}(\text{NO}_3)_2 \cdot 6\text{H}_2\text{O}$ precursor (Series B). Fig. 4 reveals agglomerated particles that suggest a poor dispersion of the Fe particles over the MgO substrate presumably due to the lack of MgFe_2O_4 phase. An average Fe particle size of 35 nm and a standard deviation of 19 nm is obtained for this sample.

To obtain detailed structural information, XPS analysis was used to elucidate the elemental composition and valence state of obtained products. The high-resolution narrow-scan XPS spectra of the O 1s, Fe 2p, and Mg 2p are illustrated in Fig. 5(a)–(d).

In the Mg 2p spectra (Fig. 5(a)), the signal could be deconvoluted into peaks at 49.4 and 50.1 eV, consistent with different environments of Mg^{2+} ions: octahedral sites (Mg_B^{2+}) in the spinel structure and Mg–O sites. By calculating the relative intensities of spectral components for Mg

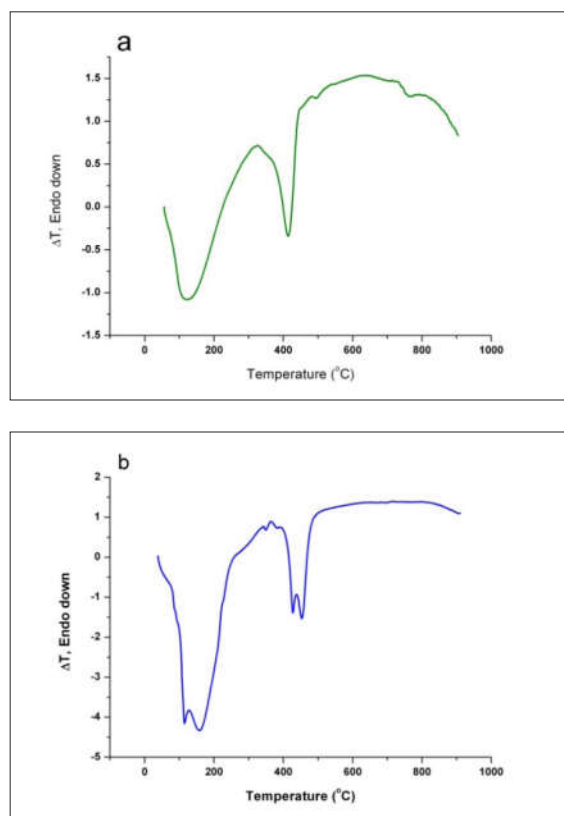


Fig. 2. a and b. DTA results in air at a heating rate of $5^{\circ}\text{C min}^{-1}$, for a mixture of catalyst and support made from series A ($\text{MgO} + \text{Fe}_2(\text{SO}_4)_3 \cdot x\text{H}_2\text{O}$) and B ($\text{Mg}(\text{NO}_3)_2 \cdot 6\text{H}_2\text{O} + \text{Fe}_2(\text{SO}_4)_3 \cdot x\text{H}_2\text{O}$), calcined at 900°C for 1 hour.



Fig. 3. (a and b): TEM bright field images, at two different magnifications, and (c): dark field STEM image and STEM/EDX maps (blue = Mg and red = Fe) for sample series A ($\text{MgO} + \text{Fe}_2(\text{SO}_4)_3 \cdot 7\text{H}_2\text{O}$), calcined at 900 °C for 1 hour.



Fig. 4. (a and b): TEM bright field images, at two different magnifications, and (c): dark field STEM image and STEM/EDX maps (blue = Mg and red = Fe) for sample series B ($\text{Mg}(\text{NO}_3)_2 \cdot 6\text{H}_2\text{O} + \text{Fe}_2(\text{SO}_4)_3 \cdot 7\text{H}_2\text{O}$), calcined at 900 °C for 1 hour.

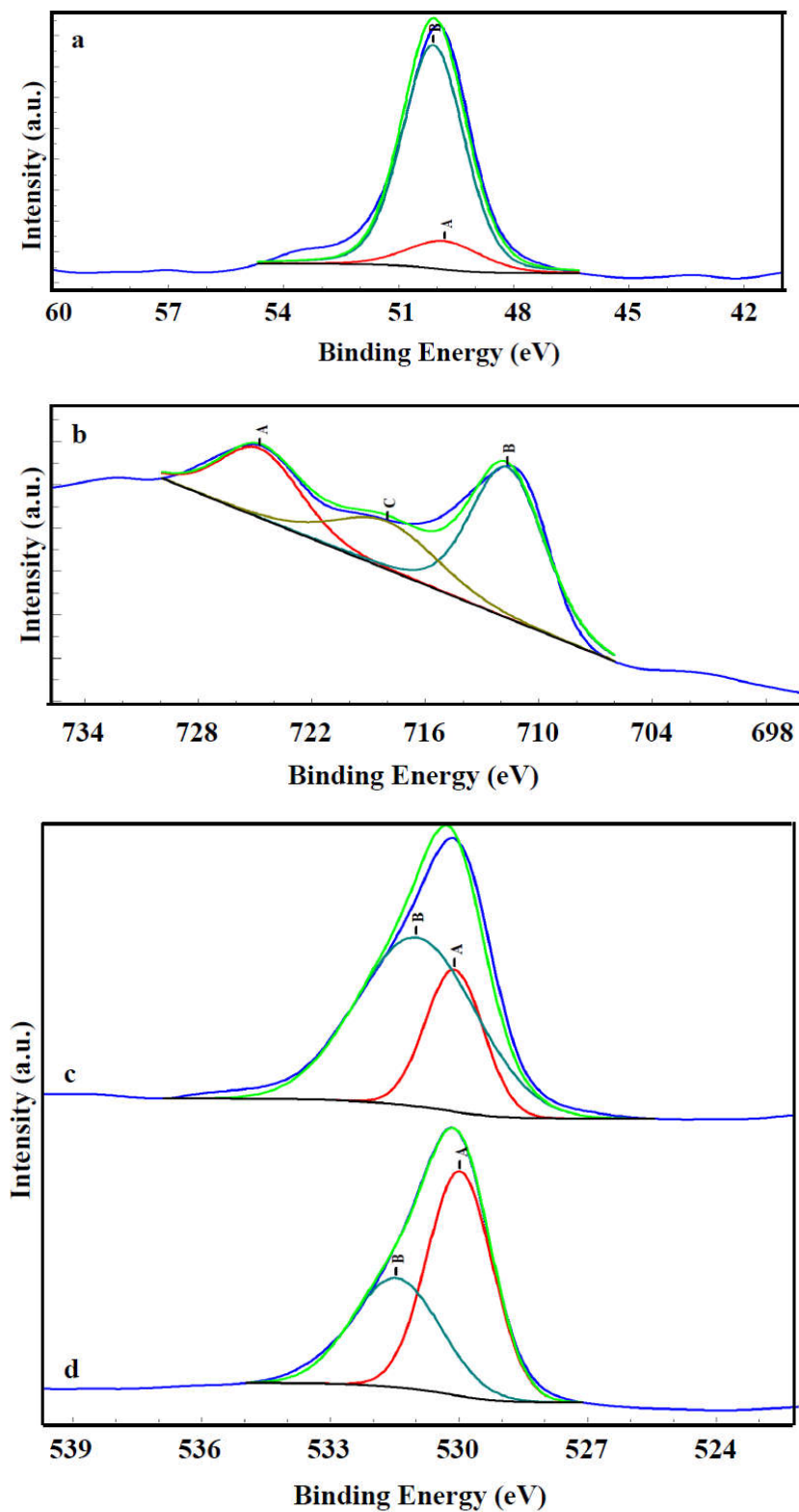


Fig. 5. (a - d): XPS spectra of MgFe_2O_4 ferrites: HRXPS spectra of Mg 2p peak (a), Fe 2p peak (b), O1s peak for sample consisting of $\text{Mg}(\text{NO}_3)_2 \cdot 6\text{H}_2\text{O}$ precursor and iron sulfate (c) and O1s peak for sample consisting of MgO precursor and iron sulfate (d).

2p, it can be concluded that most of the Mg^{2+} ions occupied Mg–O sites. The Fe 2p_{3/2} and Fe 2p_{1/2} core level peaks are clearly observed at 711.6 and 724.4 eV (Fig. 5(b)) with a satellite line at 718.5 eV corresponding to Fe^{+3} in $\gamma\text{-Fe}_2\text{O}_3$ [49]. Fig. 5 (c and d) displays the high-resolution XPS spectrum of O(1s), which can be deconvoluted into two peaks located at 529.9 and 531.8 eV. The first component is located at binding energy of 529.9 eV, which can be assigned to oxygen in the lattice (denoted as M–O), i.e., oxygen atoms that are bound to magnesium and iron atoms (Mg–O, Fe–O). The second component, at about 531.8 eV, can be assigned to metal hydroxides or hydroxyl groups (denoted as OH⁻).

Quantitative results reveal that the interaction between iron and magnesium and the formation of ferrite phase in samples with the source of magnesium oxide (Series A, Fig. 5(d)) is about 50% higher in comparison with interactions in samples which have been synthesized by using nitrate as the source (Series B, Fig. 5(c)).

The XPS analysis demonstrates that MgFe_2O_4 microspheres are successfully synthesized in both samples. However, according to XPS results, due to the low ratio of (Mg–O, Fe–O) formation in series A samples, interaction between Mg and Fe is stronger than series B samples. Therefore, it can be concluded that series A samples would be the better candidates to be employed to synthesize CNTs. These results are in agreement with our previous study [27].

4. CONCLUSION

The type of precursors employed to prepare the support for the catalyst particles had a significant influence on the morphology of the resulting support and consequently on the metal catalyst particle dispersion. Pure MgO precursors which form a higher yield of the MgFe_2O_4 phase following the calcination, resulted in a fine distribution of Fe particles over the support surface. However, by using $\text{Mg}(\text{NO}_3)_2 \cdot 6\text{H}_2\text{O}$ precursors, the amount of the synthesized MgFe_2O_4 phase was reduced resulting in agglomeration of Fe particles which could have a considerable influence on the yield and quality of CNTs.

ACKNOWLEDGMENTS

Thanks are due to Dr. Michael Ward from the University of Leeds for fruitful discussions and technical support during the using of TEM facilities.

References

1. Iijima, S., "Helical microtubules of graphitic carbon", *Nature*, 1991, 358, 56-58.
2. Krishnan, A., Dujardin, E., Ebbesen, T. W., Yianilos, P. N. and Treacy, M. M., "Young's modulus of single-walled nanotubes", *J. Phys. Rev. B*, 1998, 58, 14013-14019.
3. Dresselhaus, M. S., Dresselhaus, G., and Saito, R., "Physics of carbon nanotubes", *Carbon*, 1995, 33, 883-891.
4. Guo, T., Nikolaev, P., Thess, A., Colbert, D. T. and Smalley, R. E., "Catalytic growth of single-walled nanotubes by laser vaporization", *Chem. Phys. Lett.*, 1995, 243, 49-54.
5. Iijima, S. and Ichihashi, T., "Single-shell carbon nanotubes of 1-nm diameter", *Nature*, 1993, 363, 603-605.
6. Liu, J., Dai, H., Hafner, J. H., Colbert, D. T., Tans, S. J., Dekker, C. and Smalley, R. E., "Fullerene crop circles", *Nature* 1997, 385, 780-781.
7. Birkett, P. R., Cheetham, A. J., Eggen, B. R., Hare, J. P., Kroto, H. W., and Walton, D. R. M., "Transition metal surface decorated fullerenes as possible catalytic agents for the creation of single walled nanotubes of uniform diameter", *Chem. Phys. Lett.* 1997, 281, 111-114.
8. Rodriguez, N. M., Kim, M. S. and Baker, R. T. K., "Carbon nanofibers: a unique catalyst support medium", *J. Phys. Chem.*, 1994, 98, 13108-13111.
9. Chia-Ming, C., Yong-Ming, D., Gwo, H. J., and Jih-Mim, J., "Intermetallic catalyst for carbon nanotubes (CNTs) growth by thermal chemical vapor deposition method", *Carbon*, 2006, 44, 1808-1820.
10. Che, G., Lakshuri, B. B., Martin, C. R., Fisher, E. R. and Ruoff, R. S., "Chemical Vapor Deposition Based Synthesis of Carbon Nanotubes and Nanofibers Using a Template Method", *Chem. Mater.*, 1998, 10, 260-267.
11. Hernadi, K., Kónya, Z., Siska, A., Kiss, J., Oszkó, A., Nagy, J. B., and I. Kiricsi, "On the role of catalyst, catalyst support and their interaction in synthesis of carbon nanotubes by CCVD", *Mater. Chem. Phys.*, 2002, 77, 536-541.



12. Audier, M., Oberlin, A., and Oberlin, M., "Morphology and crystalline order in catalytic carbons", *Carbon*, 1981, 19, 217-224.
13. Hernadi, K., Fonseca, A., Nagy, J. B., Bernaerts, D., Fudala, A., and Lucas, A. A., "Catalytic synthesis of carbon nanotubes using zeolite support", *Zeolites*, 1996, 17, 416-423.
14. Esmaili, M., Khodadadi, A., Mortazavi, Y., "Catalyst support and pretreatment effects on carbon nanotubes synthesis by chemical vapor deposition of methane on iron over SiO_2 , Al_2O_3 or MgO , *Chem. Reactor Eng.*, 2009, 7, A36.
15. Jodin, L., Dupuis, A., Rouvière, E., and Reiss, P., "Influence of the Catalyst Type on the Growth of Carbon Nanotubes via Methane Chemical Vapor Deposition", *J. Phys. Chem. B*, 2006, 110, 7328-7333.
16. Magrez, A., Seo, J. W., Smajda, R., Mionic, M. and Forró, L., "Catalytic CVD Synthesis of Carbon Nanotubes: Towards High Yield and Low Temperature Growth", *Mater.*, 2010, 3, 4871-4891.
17. Jourdain, V., Bichara, C., "Current understanding of the growth of carbon nanotubes in catalytic chemical vapour deposition", *Carbon*, 2013, 58, 2-39.
18. Kumar, M. and Ando, Y., "Chemical Vapor Deposition of Carbon Nanotubes: A Review on Growth Mechanism and Mass Production", *J. Nanosci. Nanotechnol.*, 2010, 10, 3739-3758.
19. Wang, Y., Luo, Z., Li, B., Ho, P. S., Yao, Z., Shi, L., Bryan, E. N., Nemanich, R. J., Comparison study of catalyst nanoparticle formation and carbon nanotube growth: Support effect, *J. Appl. Phys.*, 2007, 101, 124310.
20. Ur Rashid, H., Yu, K., Umar, M. N., Anjum, M. N., Khan, K., Ahmad, N. and Tariq, M. Jan, "Catalyst role in chemical vapor deposition (CVD) process: A review", *Rev. Adv. Mater. Sci.*, 2015, 40, 235-248.
21. Arcos, T., Garnier, M. G., Seo, J. W., Oelhafen, P., Thommen, V., and Mathys, D., "The Influence of Catalyst Chemical State and Morphology on Carbon Nanotube Growth", *J. Phys. Chem. B*, 2004, 108, 7728-7734.
22. Kharlamova, M. V., "Investigation of growth dynamics of carbon nanotubes", *Beilstein J. Nanotechnol.*, 2017, 8, 826-856.
23. Che, G., Lakshuri, B. B., Martin, C. R., Fisher, E. R. and Ruoff, R. S., "Chemical Vapor Deposition Based Synthesis of Carbon Nanotubes and Nanofibers Using a Template Method", *Chem. Mater.*, 1998, 10, 260-267.
24. Dupuis, A. C., "The catalyst in the CCVD of carbon nanotubes—a review", *Prog. Mater. Sci.*, 2005, 50, 929-961.
25. Ning, G., Wei, F., Wen, Q., Luo, G., Wang, Y. and Jin, Y., "Improvement of Fe/MgO Catalysts by Calcination for the Growth of Single- and Double-Walled Carbon Nanotubes", *J. Phys. Chem. B*, 2006, 110, 1201-1205.
26. Coquay, P., Peigney, A., Grave, E. D., Vandenberghe, R. E. and Laurent, C., "Carbon Nanotubes by a CVD Method. Part II: Formation of Nanotubes from (Mg, Fe)O", *J. Phys. Chem. B*, 2002, 106, 13186 -13198.
27. Palizdar, M., Ahgabayazadeh, R., Mirhabibi, A., Brydson, R. and Pilehvari, S., "Investigation of Fe/MgO Catalyst Support Precursors for the Chemical Vapour Deposition Growth of Carbon Nanotubes", *J. Nanosci. Nanotechnol.*, 2011, 11, 5345-5351.
28. Gulková, D., Šolcová, O., Zdražil, M., "Preparation of MgO catalytic support in shaped mesoporous high surface area form", *Microporous and Mesoporous Mater.*, 2004, 76, 137-149.
29. Ago, H., Nakamura, K., Uehara, N. and Tsuji, M., "Roles of Metal-Support Interaction in Growth of Single- and Double-Walled Carbon Nanotubes Studied with Diameter-Controlled Iron Particles Supported on MgO", *J. Phys. Chem. B*, 2004, 108, 18908-18915.
30. Li, W. Z., Wen, J. G., Sennett, M., Ren, Z. F., "Clean double-walled carbon nanotubes synthesized by CVD", *Chem. Phys. Lett.*, 2003, 368, 299-306.
31. He, M., Jiang, H., Liu, B., Fedotov, P. V., Chernov, A. I., Obratsova, E. D., Cavalca, F., Wagner, J. B., Hansen, T. W., Anoshkin, I. V., Obratsova, E. A., Belkin, A. V., Sairanen, E., Nasibulin, A. G., Lehtonen, J. and Kauppinen, E. I., "Chiral-Selective Growth of Single-Walled Carbon Nanotubes on Lattice-Mismatched Epitaxial Cobalt Nanoparticles", *Sci. Reports*, 2013, 3, 1460.
32. Qingwen, L., Hao, Y., Yan, C., Jin, Z. and Zhongfan, L., "A scalable CVD synthesis of high-purity single-walled carbon nanotubes with porous MgO as support material", *J. Mater. Chem.*, 2002, 12, 1179-1183.
33. Kumar, M., "Carbon Nanotube Synthesis and Growth Mechanism", *Intechopen*, 2011.
34. Ago, H., Uehara, N., Yoshihara, N., Tsuji, M., Yumura, M., Tomonaga, N., Setoguchi, T., "Gas analysis of the CVD process for high yield growth of carbon nanotubes over metal-supported catalysts", *Carbon*, 2006, 44, 2912-2918.
35. Zheng, B., Lu, C., Gu, G., Makarovski, A., Finkelstein, G. and Liu, J., "Efficient CVD Growth

- of Single-Walled Carbon Nanotubes on Surfaces Using Carbon Monoxide Precursor”, *nano lett.*, 2002,2, 895-898.
36. Kukovecz, A., Mehn, D., Nemes-Nagy, E., Szabo, R. and Kiricsi, I., “Optimization of CCVD Synthesis Conditions for Single-wall Carbon Nanotubes by Statistical Design of Experiments (DoE)”, *Carbon*, 2005, 43, 2842-2849.
 37. Kathyayini, H., Nagaraju, N., Fonseca, A. and Nagy, J. B., “Catalytic activity of Fe, Co, and Fe/Co supported on Ca and Mg oxides, hydroxides and carbonates in the synthesis of carbon nanotubes”, *J. Mol. Catal. A: Chem.*, 2004, 223, 129-136.
 38. Qiu, J., An, Y., Zhao, Z., Li, Y. and Zhou, Y., “Catalytic synthesis of single-walled carbon nanotubes from coal gas by chemical vapor deposition method”, *Fuel Process. Technol.*, 2004, 85, 913-920.
 39. Kong, J., Cassell, A. M., and Dai, H., “Chemical vapor deposition of methane for single-walled carbon nanotubes”, *Chem. Phys. Lett.*, 1998, 292, 567-574.
 40. Kuczynski, G. C., Ferrites, “In proceedings of the international conference on ferrites”, Kyoto, Japan, University of Tokyo press, 1971, 87, 331-315.
 41. Wagner, C., “Diffusion and high temperature oxidation of metals”, in *Atom Movements*, ASM, Cleveland, USA, 1951, 153.
 42. Rapp, R. A., “The high temperature oxidation of metals forming cation-diffusing scales”, *Metall. Mater. Trans. B*, 1984,15, 195-212.
 43. Schmalzried, H., “Reaktionsmechanismen der Spinellbildung im festen Zustand”, *Z. Physik. Chem.*, 1962,33 , 111-128.
 44. Economos, G., “In kinetics of high temperature process”, M.I.T. Press, Cambridge, 1959, 243.
 45. Blackman, L. C. F., “On the Formation of Fe^{2+} in the System $\text{MgO-Fe}_2\text{O}_3\text{-MgFe}_2\text{O}_4$ at High Temperatures”, *J. Am. Ceram. Soc.*, 1959, 42, 143-145.
 46. Palizdar, M., Comyn, T. P., Palizdar, Y. and Bell, A. J., “Electron Backscattered Diffraction of MonoCrystalline Bismuth Titanate”, *J. Am. Ceram. Soc.*, 2010, 93(11), 3604-3606.
 47. Christahl, M. and Anton, S., “The thermal properties of group II metal hydroxides and of the octa-hydrates of strontium and barium hydroxide”, *Int. J. Hydrogen Energ.* 1984, 9 , 603-607.
 48. Petkova, V. and Pelovski , Y., “Comparative DSC study on thermal decomposition of iron sulphates”, *J. Therm. Anal. Calorim.*, 2009, 93, 847.
 49. Yan, Z., Gao, J., Li, Y., Zhang, M., Guo, M., “Hydrothermal synthesis and structure evolution of metal-doped magnesium ferrite from saprolite lat-erite”, *RSC Adv.*, 2015, 5, 92778-92787.